A Microstructural and Wear Resistance Study of Stainless Steel-Ag Coatings Produced through Magnetron Sputtering

Claudia L. España P. [1], Abel A. C. Recco [2] and Jhon J. Olaya [1,*]

[1] Department of Mechanical and Mechatronics Engineering, Universidad Nacional de Colombia, Bogotá 111321, Colombia; clespanap@unal.edu.co

[2] Physics Department, Santa Catarina State University, UDESC, Joinville 89219-710, Brazil; abel.recco@udesc.br

* Correspondence: jjolayaf@unal.edu.co; Tel.: +57-1-316-5000-11208

check for updates

Abstract: This paper presents a study of the tribological properties of stainless steel coatings with varying Ag contents, deposited via magnetron sputtering. The growth of the coatings was done in Ar and Ar + N_2 atmospheres in order to change the crystalline phase in the coating. The analysis of the chemical composition was performed using energy-dispersive X-ray spectroscopy (EDS) and the structural analysis was performed via X-ray diffraction (XRD). The adhesive wear resistance and the friction coefficient were evaluated using the ball-on-disk test with a ball of alumina. The coatings' adhesion was measured with a scratch tester and the mechanical properties were evaluated with a nanoindenter. The morphology of the films and the wear track were characterized via scanning electron microscopy (SEM). By means of XRD, phases corresponding to the body-centred cubic (BCC) structure were found for the coatings deposited in an inert atmosphere and face-centred cubic (FCC) for those deposited in a reactive atmosphere. A more compact morphology was observed in coatings with a higher silver content. The values of the hardness increased with an increase in the silver content and the presence of nitrogen in the coatings. In the wear traces, mainly mechanisms of oxidative and adhesive wear and plastic deformation were found. The coefficient of friction decreased with an increase of silver in the coatings, whereas the wear rate decreased.

Keywords: stainless steel coating; sputtering; wear; adhesion; friction; structure

1. Introduction

Stainless steels have good resistance to corrosion, high resistance to cold work and good formability. One of the stainless steels used in the biomedical, automotive, naval and aeronautical industries is AISI 316L austenitic stainless steel, since it has good corrosion resistance due to the presence of a thin film of chromium oxide on its surface, known as a passive film [1–5]. However, its low mechanical resistance is sometimes not enough for mechanical applications, causing fractures in structural elements due to mechanical stress and fatigue [6,7]. In view of this, it is important to improve the durability of AISI 316L steel by increasing its hardness and wear resistance [8].

The deposition of coatings on steel allows an improvement in its properties such as hardness and resistance to corrosion, wear and fatigue, among others, in comparison with bulk austenitic stainless steels [9–11]. Stainless steel-based coatings deposited by means of the sputtering technique have been characterized in different investigations. It has been found that this type of coating has a chemical composition similar to that of austenitic stainless steel targets; however, a variation in the structure has been found; for instance, a BCC structure is produced for coatings deposited in inert atmospheres (Ar), while for reactive atmospheres (Ar + N_2), coatings are obtained with a mixture of FCC and BCC

phases or only FCC, depending on the amount of nitrogen and the substrate temperature used in the process [10,11]. At the same time, in recent years silver (Ag) has become a material widely used as a dopant in thin films, due to its antibacterial activity, hence its use for the purpose of supplying antibacterial properties to biomedical devices. In coatings, silver can form nanoparticles (AgNPs), improving the antimicrobial activity of biomaterials and reducing the coefficient of friction. Among the medical applications of this type of material, coated or integrated with AgNPs to avoid bacterial growth, are wound dressings, contraceptive devices, surgical instruments and external prostheses [12–14]. The deposition of coatings containing silver has been a subject of interest in applications where materials with good tribological and antibacterial properties are required. Evidence has been shown of a tendency to increase the durability of the different types of compounds that contain silver, because in many cases properties such as the wear resistance and the coefficient of friction are improved, which can be attributed to the possible action of silver as a solid lubricant on the surface of the coatings, thus reducing wear [15–17].

We investigated the effect of silver on the microstructure and the mechanical and tribological properties of stainless steel films with varying silver content that were deposited by means of magnetron sputtering on stainless steel substrates. The growth of the coatings was done in Ar and Ar + N_2 atmospheres in order to change the crystalline phase in the coating.

2. Materials and Methods

Stainless steel coatings were deposited by means of DC magnetron sputtering. The discharge was done with a 316L stainless steel target of 10 cm in diameter and 0.64 cm in thickness, where 1, 2 and 4 pieces of Ag of 4 mm × 4 mm were added to the surface of the target. The target was facing up so that the Ag target sat on top of the SS316 target by gravitational force. The base pressure was 9×10^{-3} Pa and the working pressure was fixed at 0.2 Pa. The deposition gas was composed of argon (purity 99.9%) and nitrogen (purity 99.9%) with flux 1.2 and 0.8 sccm, respectively. The power density was 7 W/cm^2. The substrate temperature was 300 °C and the substrate-target distance was maintained at 6 cm. The coatings were deposited on AISI 316L substrates, which were previously sanded with abrasive paper from 180 to 2000 and polished with cloth and 2.0 µm alumina suspension. To remove alumina particles during the final polishing, an amphoteric surfactant was used. Finally, in order to reduce organic impurities, especially fats, the samples were cleaned with acetone and 2-propanol in ultrasound for 10 min. The thickness of the deposited films was measured by means of a Bruker DektakXT profilometer (Billerica, MA, USA). To perform the thickness measurements, silicon substrates were used, on each of which were placed pieces of silicon in order to generate a step during the deposition of the coatings. The thickness of the deposited thin films was between 3.0 and 4.0 µm, with deposition times of 28 and 32 min for inert and reactive atmospheres, respectively. The coatings were designated as shown in Table 1 according to the amount of Ag pieces used and the atmosphere in which they were deposited.

Table 1. Stainless steel coatings deposited with and without Ag pieces and in inert and reactive atmospheres.

Coating	Silver Pieces	Atmosphere
Ar0Ag	0	Ar
Ar1Ag	1	Ar
Ar4Ag	4	Ar
ArN0Ag	0	Ar + N_2
ArN1Ag	1	Ar + N_2
ArN4Ag	4	Ar + N_2

To study the microstructure, an X'Pert PRO PANalytical grazing incidence X-ray diffraction system (GI-XRD) (Panalytical, Almelo, The Netherlands) was used. The incidence angle was set to

1°, while the swept angle was varied from 35° to 85° in 2θ mode (scanning step of 0.02°), with Cu Kα (1.5418 Å) radiation operating at 45 kV and 40 mA. The grain size of the crystalline phases was determined by the Scherrer formula, as shown in Equation (1).

$$\text{Grain size} = \frac{k\lambda}{B\cos\theta} \tag{1}$$

where k is a constant related to the shape factor (0.94), λ is the X-ray wavelength used in the experiment, *B* is the peak broadening at half maximum intensity in radians (taking into account the subtraction of the experimental error of the measuring equipment, Bexp) and θ is the Bragg angle.

The percentage of lattice distortion or strain (ε), which is directly proportional to the residual stress, was estimated from the difference between the measured lattice spacing and the bulk parameter lattice spacing. The lattice parameter was calculated from the position of the (110), (200) and (111) Bragg reflections in the XRD spectra. The morphology of the films was studied by means of scanning electron microscopy (SEM, 6701F-JEOL, Tokyo, Japan) and the chemical composition was studied at one spot, via an energy-dispersive X-ray system (Shimadzu EDX-720, Tokyo, Japan), which allowed detecting elements from Na ($Z = 11$) to U ($Z = 90$). EDS spectra were collected from different locations on a homogeneous zone, where each single scan area was approximately 10×10 mm^2.

Hardness measurements were done with a CTER Nano-Micro nanoindenter (CTER, San Jose, CA, USA). For the hardness test, a Berkovich diamond tip with a radius of 200 nm was used, applying a maximum load of 10 μN in all samples in order to measure hardness (*H*) and reduced modulus (E_r). To separate the contributions of the substrate properties in the film measurements, the indentation depth was below 10% of film thickness. From the reduced modulus, the elastic modulus of the film was calculated using Equation (2) [18].

$$\frac{1}{E_r} = \frac{(1-\nu_f^2)}{E_f} + \frac{(1-\nu_i^2)}{E_i} \tag{2}$$

where E_r is the reduced modulus, E_i and ν_i are the elastic modulus (1140 GPa) and Poisson's ratio (0.07) of the Berkovich indenter, respectively and E_f and ν_f are the elastic modulus and Poisson's ratio (0.29) of the film, respectively.

The pin-on-disc method was carried out to determine the wear resistance. The test was done using a CETR-UMT-2-110 tribometer (CTER, San Jose, CA, USA) with a stationary pin in air under ambient laboratory conditions. A 6 mm diameter alumina ball was used under a normal load of 1 N and 2 N and a sliding speed of 10 and 50 mm/s for 20 s. In order to obtain a stable coefficient of friction value and determine the wear rate of the coatings, additional tests were carried out under a load of 1 N at a speed of 10 mm/s for 10 min. The wear volume (W_v) of the films was calculated according to ASTM G99-17 [19]. The wear track cross profile was measured at least four points of the wear track with a Dektak 150 profilometer (Bruker, Billerica, MA, USA) in order to obtain an average of the wear track width. After the test, the wear tracks were examined using a Bruker contour GT optical profilometer. The wear products were chemically analysed using energy-dispersive X-ray spectroscopy (EDS). The wear rate (W_s) was calculated according to Archard's equation, Equation (3) [20], where *F* is the normal load (N) and *L* is the sliding length (mm). The wear rate is reported in mm^3/Nm.

$$W_s = \frac{W_v}{F \cdot L} \tag{3}$$

The adherence of the coating was measured by means of the scratch test technique with a CSM Instruments model Revetest Xpress. For the test, a progressive load was applied from 1 to 60 N. Then the scratch tracks were characterized by means of optical microscopy in order to measure the critical loads of the coatings.

3. Results

The XRD patterns obtained for the stainless steel coatings deposited in an Ar atmosphere are shown in Figure 1. A body-centred cubic structure can be seen, with mixed orientation, where the peaks were indexed as (110), (200) and (211). The BCC phase is associated with the ferritic structure of stainless steel, commonly obtained when the atmosphere of the sputtering process is composed only of Ar, as has been found by other researchers [9–11]. Furthermore, peaks related to the presence of the FCC structure of silver in Ar1Ag and Ar4Ag coatings can be seen [17,21,22]. In the XRD pattern of the target, a face-centred cubic structure with mixed orientation can be seen, where the peaks were indexed as (111), (200) and (220).
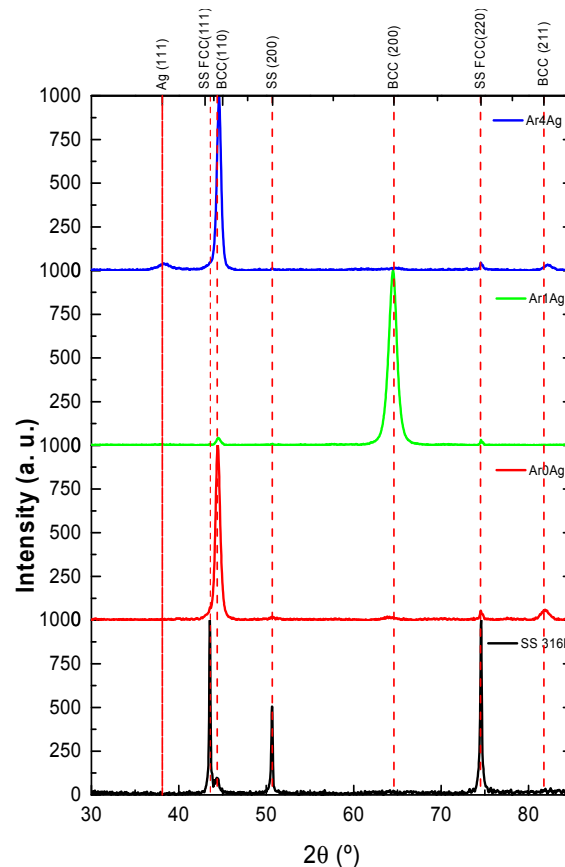

Figure 1. X-ray diffraction (XRD) diffraction patterns of stainless steel coatings deposited in Ar atmosphere.

Figure 2 shows the XRD patterns corresponding to the coatings deposited in the reactive atmosphere (Ar + N$_2$). A face-centred cubic (FCC) structure can be seen, with a (200) preferential orientation in the sample without Ag (ArN0Ag), because the nitrogen tends to stabilize the FCC structure by broadening the gamma loop in the iron-carbon equilibrium diagram, which has been reported by other researchers [9–11]. However, with the addition of Ag, the (111) signal appears and for the sample with highest Ag content (the ArN4Ag sample) the (111) orientation increases and the (200) disappears. In other studies, it has been reported that the addition of high silver content to different types of materials tends to increase the amorphization of the matrix, which can be attributed to the interruption of the growth of the crystalline phase by the nucleation of Ag nanocrystals at the grain boundaries [22–24].

Table 2 shows the results regarding the size of the crystallite, the percentage of deformation and the lattice parameters. The coatings deposited in a nitrogen atmosphere have a smaller crystallite size and higher values of deformation and lattice parameters. This could be attributed to the inclusion

of nitrogen in the octahedral sites of the austenite lattice, generating a lattice distortion as well as expansion of the FCC lattice [9,10,25,26].
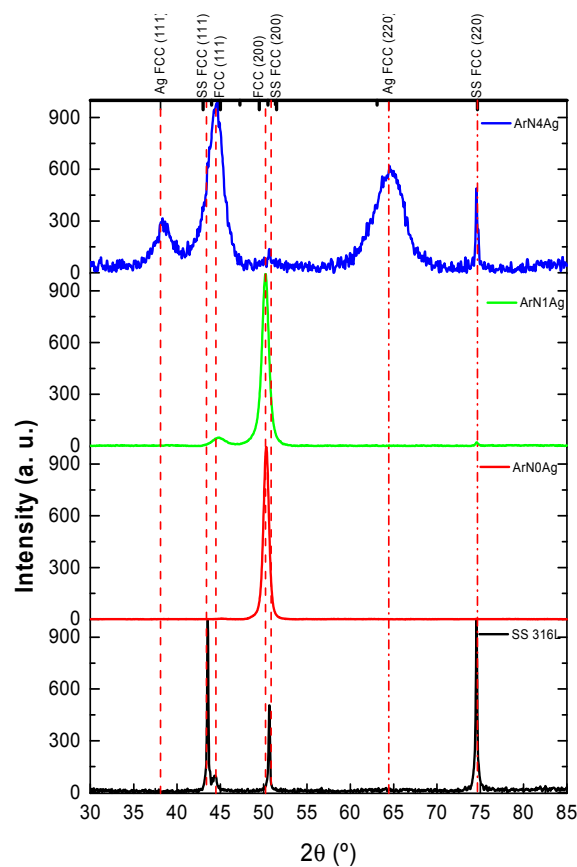

Figure 2. XRD diffraction patterns of stainless steel coatings deposited in Ar + N$_2$ atmosphere.

Table 2. Results of the size of the crystallite (*D*), percentage of deformation (*ε*) and lattice parameter (*a*).

Coating	Phase	Reflection (h k l)	D (nm)	ε	a (nm)
Ar0Ag	BCC	110	15.45	0.10	0.288
Ar1Ag	BCC	200	8.28	0.31	0.289
		110	19.24	0.08	0.288
Ar4Ag	BCC	110	16.46	0.09	0.287
ArN0Ag	FCC	200	12.93	0.15	0.363
ArN1Ag	FCC	200	9.69	0.19	0.363
AgN4Ag	FCC	111	4.24	0.38	0.353

Figure 3 shows the surface morphology and cross section of the stainless steel coating with the highest Ag content (sample Ar4Ag) deposited in an inert atmosphere, where a homogeneous surface, without the presence of defects and a columnar structure that is in accordance with zone I of the Thornton model [27] can be seen. Figure 4 shows the microstructure of the AgN4Ag sample deposited in an atmosphere of nitrogen, in which is seen a more compact morphology with less columnar structure, which could be associated with the T zone structure of the Thornton model [27]. This can be attributed to a combination of the nitrogen in the plasma and the highest percentage of silver deposited in this coating, which can be segregated at the grain boundaries and columns, interrupting the columnar growth by decreasing the size and number of voids between the columns. Also, the Ag phase is dispersed in the steel crystal, grain growth is inhibited and grain refinement is promoted [28].
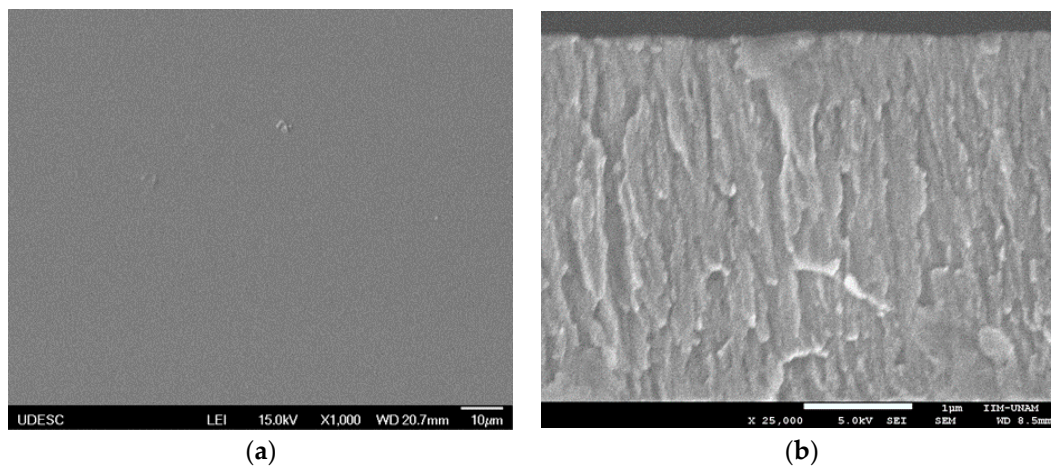
Figure 3. Scanning electron microscopy (SEM) micrographs of Ar4Ag films: (**a**) surface; (**b**) cross-section.
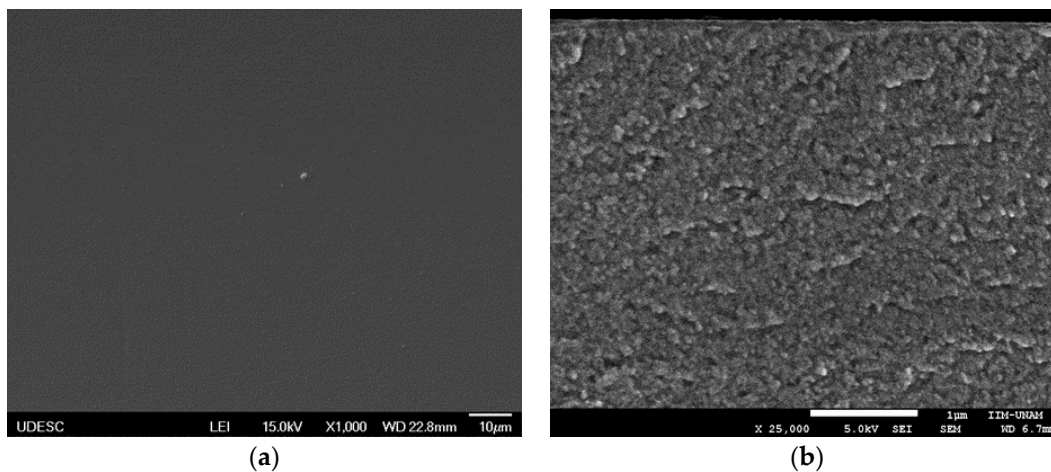

Figure 4. SEM micrographs of ArN4Ag films: (**a**) surface; (**b**) cross-section.

The chemical composition and the mechanic properties are shown in Table 3. The presence of the elements Fe, Cr, Ni, Mn and Mo can be seen, which are commonly found in this type of coating. In addition, there is a slight deviation with respect to the target's chemical composition, due to the difference in sputtering yield between its elements and because the pieces of Ag were added to the surface of the target. Also, an increase in Ag up to 5.25 at.% and 13.06 at.% can be seen in the inert and reactive atmospheres, respectively.

Table 3. Mechanical properties and chemical composition of deposited coatings.

Coating	Hardness (GPa)	Elastic Module (GPa)	H/E	H^3/E^2 (GPa)	Chemical Composition (at.%)					
					Cr	Fe	Ni	Mn	Mo	Ag
Ar0Ag	8.1 ± 0.8	211 ± 14	$0.039 \pm 6.4 \times 10^{-5}$	$0.012 \pm 5.1 \times 10^{-5}$	16.3	69.1	9.6	2.8	2.3	0.0
Ar1Ag	8.6 ± 0.4	210 ± 12	$0.041 \pm 4.2 \times 10^{-5}$	$0.014 \pm 3.6 \times 10^{-5}$	16.3	68.1	9.8	2.6	2.2	1.0
Ar4Ag	10 ± 0.5	242 ± 15	$0.042 \pm 4.7 \times 10^{-5}$	$0.018 \pm 4.9 \times 10^{-5}$	15.7	64.8	9.5	2.6	2.2	5.2
ArN0Ag	8.2 ± 0.3	187 ± 15	$0.044 \pm 5.1 \times 10^{-5}$	$0.016 \pm 4.3 \times 10^{-5}$	16.4	68.6	9.8	3.1	2.2	0.0
ArN1Ag	9.9 ± 0.3	196 ± 8	$0.051 \pm 3.6 \times 10^{-5}$	$0.025 \pm 4.3 \times 10^{-5}$	17.2	67.7	9.5	3.0	2.2	0.5
ArN4Ag	13.2 ± 0.5	214 ± 7	$0.062 \pm 4.4 \times 10^{-5}$	$0.050 \pm 8.9 \times 10^{-5}$	14.4	59.5	8.7	2.4	2.0	13.1
Target 316L	–	–	–	–	17.4	65.6	8.9	3.8	4.2	0.0
Substrate 316L	2.8 ± 0.3	189 ± 15	$0.014 \pm 2.7 \times 10^{-5}$	$0.001 \pm 2.9 \times 10^{-6}$	16.4	69.9	10.1	1.5	2.1	0.0

In Table 3, high values of hardness (values up to 8 GPa) also can be seen in the deposited coatings in comparison with the substrate. However, there was no significant increase with the addition of Ag. It can be seen that the hardness has higher values in the case of coatings produced in a

reactive atmosphere, which can be attributed to the fact that the use of nitrogen tends to stabilize the austenitic phase of stainless steels. There was an increase in the lattice parameter and the percentage of deformation due to the supersaturation of nitrogen in the austenitic structure, also known as expanded austenite [10]. Based on the Hall-Petch relation, the hardness can increase with the decrease of the grain size and the increase in hardness is due to the effect of fine grain strengthening. On the other hand, the results of the H/E and H^3/E^2 ratio, where H is the hardness and E the elastic modulus of the coatings, indicate that the coatings with the highest silver content deposited in a nitrogen atmosphere exhibited higher values of these ratios, indicating a highly elastic behaviour [29] and resistance to plastic deformation [30].

Figure 5 shows the track obtained by means of the scratch test technique in coatings deposited in the absence of nitrogen. In general, the coatings have good adherence without the formation of cracks on the track; however, pile-up failure can be seen at the edges of the scratch. Also, a large part of the material is dragged by the indenter and located on the sides of the track, which is associated with stick-slip effects. Plastic deformation phenomena and material removal can be seen, mainly due to micro-cutting mechanisms, with an absence of adhesive or cohesive faults [31,32]. Similar behaviour is seen for the coatings deposited in the presence of nitrogen (see Figure 6). However, in the case of the ArN4Ag coating, there is a severe case of spallation phenomena, which is characterized by large regions of coatings with low adhesion forces, coating detachment, adhesive failure and the absence of cohesive failure [33]. It was determined that the critical load (L_c) at which the failure occurred in this coating was 2.81 N.
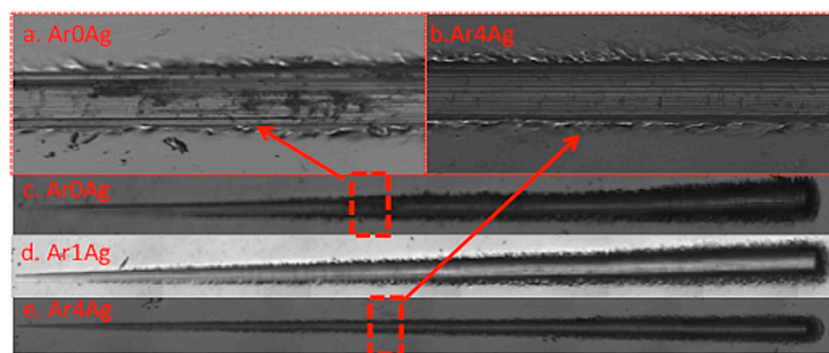

Figure 5. Micrographs of the wear track produced by the scratch tester in coatings deposited in an inert atmosphere: (**a**,**c**) Ar0Ag film; (**b**,**e**) Ar4Ag film; (**d**) Ar1Ag film.
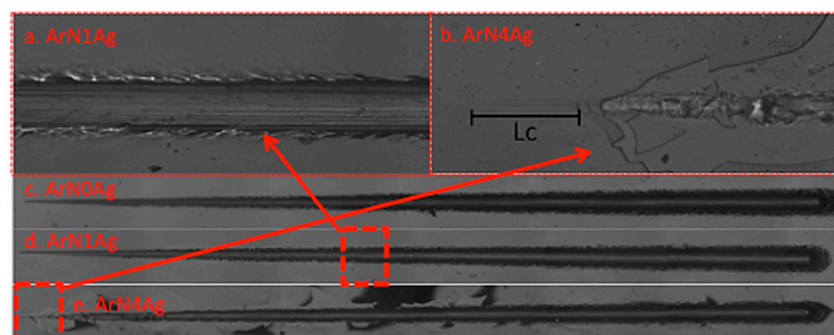

Figure 6. Micrographs of the wear track produced by the scratch tester in coatings deposited in a reactive atmosphere: (**a**,**d**) ArN1Ag; (**b**,**e**) ArN4Ag; (**c**) ArN0Ag.

The coefficient of friction (COF) of the coatings is presented in Figure 7. The coefficient of friction in the produced coatings was reduced in comparison with the substrate. It can be seen that there are no significant changes in the COF value in the coatings deposited in the absence of nitrogen (Figure 7a). As shown, the average COF of the film without Ag was 0.5 but a slight increase in the COF was

observed with the change in silver content until it reached 0.54 for the Ar4Ag sample. On the other hand, in the coatings deposited in a reactive atmosphere (Figure 7b), there was a tendency to decrease the COF with an increase in the silver content. As shown, the average COF was 0.5. However, the average COF for Ag films decreases gradually and reaches 0.35 in the ArN4Ag sample. This behaviour can be attributed to a good solid lubricant, Ag, which allows lubricating the wear tracks of the coating and friction pairs, so the sliding between the two surfaces tends to be facilitated, lowering the COF of the film. The quality of silver as a solid lubricant depends on its ability to segregate and hold during a certain number of cycles on the surface, so if the segregation of silver is low, the wear rate will not be affected but if the segregation is high, the wear rate is influenced by the time it takes for the silver to run out, since once exhausted the solid lubrication ability of the film is reduced and the surface has an unstable porous structure, causing failure and an increase in the wear rate [15,16].
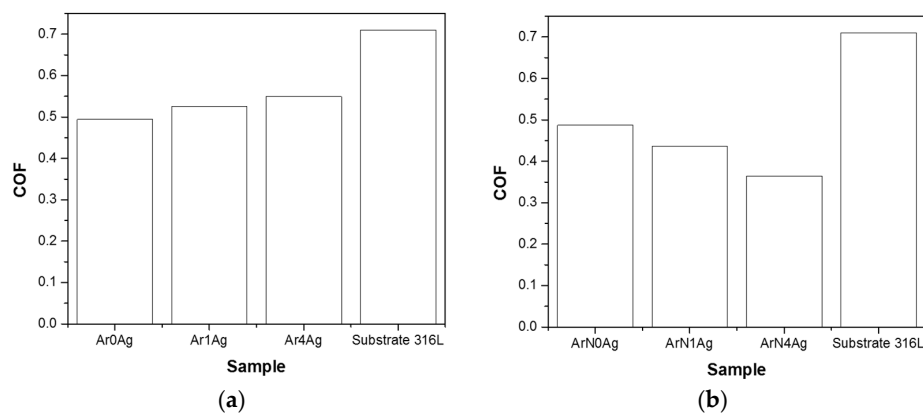

Figure 7. Values of coefficient of friction (COF) of the deposited coatings: (**a**) inert atmosphere; (**b**) reactive atmosphere.

Figure 8 shows the results of the wear rate in the produced coatings. In general, the wear rates in the produced coatings were reduced in comparison with the substrate, which is associated with the significant increase in the hardness of the coatings. Coatings deposited in the presence of nitrogen had lower values of wear rate, possibly attributable to the fact that this group has the highest values of hardness and resistance to plastic deformation. However, it can also be seen that an increase in the silver content in the film produced a higher value of the wear rate, possibly due to an increase in the fragility of the material, loss of adhesion, Ag debris and Ag aggregates formed on the wear tracks. For example, in DLC coatings doped with silver, similar results were found: a decrease in the rate of wear and COF for silver contents between 4.3% and 10.6%. This was attributed to the presence of Ag nanograins, while higher levels of Ag result in a detriment to the tribological properties of the coatings [34,35]. Therefore, Ag aggregates on the wear surface during the sliding process are forming an Ag layer on the counterpart, which may be responsible for the increased wear rate in relation to the reference coating. ZrN/Ag films also showed a decrease in the COF and an increase in the wear rate with a rise in the amount of Ag [28,36]. With an increase in the Ag content in the film, a large amount of the soft Ag phase in the film during the friction experiment is separated from the abrasive surface by the sliding of the friction pair and wear is formed, resulting in the film's wear rate increasing gradually with the Ag content. However, due to the low shear strength of Ag, in the friction process Ag easily breaks away from the wear surface with the friction of the sliding, thus forming debris, resulting in an increase in the wear rate. In addition, more and more Ag diffuses to the surface as the ambient temperature increases, forming voids inside the film which are easily worn under the pressure of the friction pair [28,35].
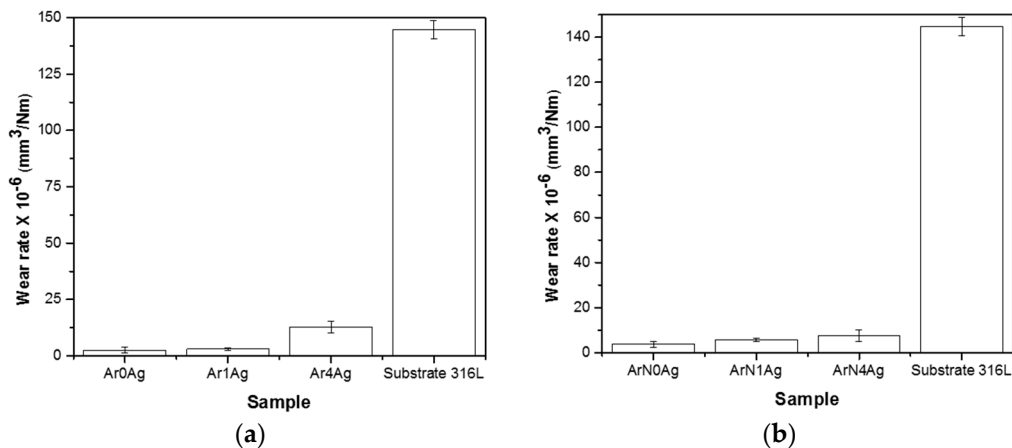
Figure 8. Values of wear rate of the coating deposited: (**a**) inert atmosphere; (**b**) reactive atmosphere.

Figures 9 and 10 show the SEM images of the worn surfaces for samples without Ag and those with higher Ag content and Table 4 shows the chemical composition through EDS of the wear tracks. A mechanism of oxidative wear can be seen for all coatings. This tribo-film is characterized by the presence of oxidized residues on the worn surface, as well as the presence of some scratches and residues of Ag, causing abrasion wear mechanisms [36]. Tribooxidation was a general phenomenon in the wear test at room temperature.
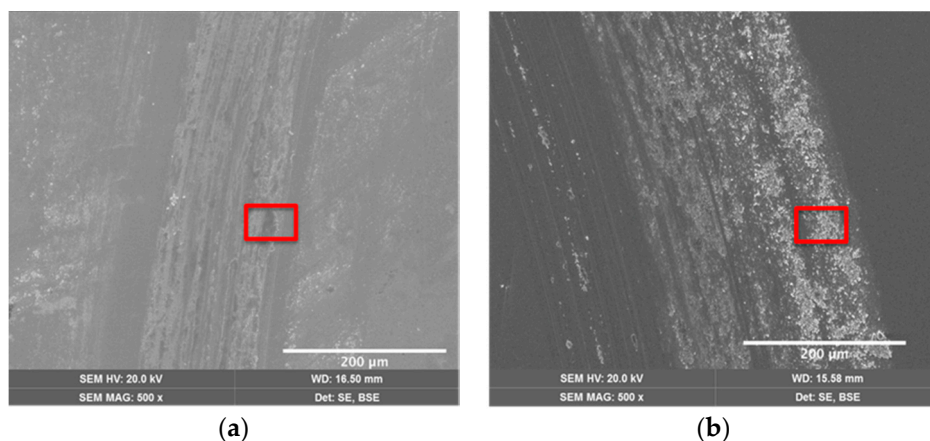

Figure 9. SEM images of wear tracks of coatings deposited in inert atmosphere: (**a**) sample Ar0Ag; (**b**) sample Ar4Ag.
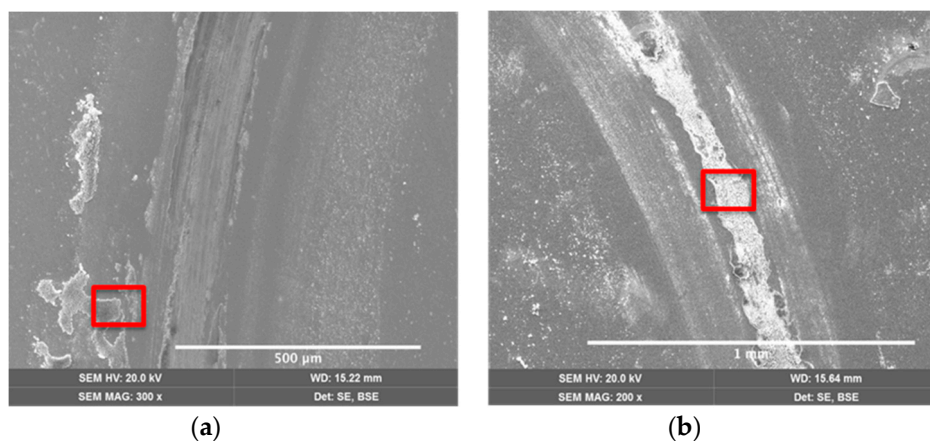

Figure 10. SEM images of wear tracks of coatings deposited in a reactive atmosphere: (**a**) ArN0Ag sample; (**b**) ArN4Ag sample.

Table 4. Results by means of the energy dispersive X-ray spectroscopy (EDS) analyses of wear tracks.

Coating	Chemical Composition (at.%)						
	Fe	Cr	Ni	O	Mn	Al	Ag
Ar0Ag	55.0	13.3	6.3	24.1	0.4	1.0	–
Ar4Ag	40.3	10.1	5.0	42.6	0.3	–	0.3
ArN0Ag	48.2	12.4	6.1	32.8	0.5	–	–
ArN4Ag	32.8	8.5	3.9	52.6	0.3	–	1.9

The coatings deposited in the reactive atmosphere (Figure 10) exhibited greater evidence of oxidative wear, according to the results of the EDS analysis (Table 4), where high percentages of oxygen can be seen in the evaluation of the chemical composition carried out on the wear tracks [25]. The plastic deformation and oxidative wear in these films can generally be attributed to the high concentration of pressure on the surface, causing a local increase in temperature, thus generating oxidation processes during wear [17]. However, delamination occurred in the coatings with a high silver content (Figure 10b). The delamination behaviour of coatings doped with Ag has been reported in other investigations for high silver contents (13.1 at.%) [16,35,36].

4. Conclusions

Stainless steel coatings with varying Ag contents were deposited in inert (Ar) and reactive (Ar and N_2) atmospheres by means of magnetron sputtering and their structural, mechanical and tribological properties were studied. The study concludes the following:

BCC and FCC microstructures were exhibited by the coatings deposited in inert and reactive atmospheres, respectively. As for coatings deposited with silver, the FCC structure of silver was also evident. The coatings deposited in a nitrogen atmosphere and with a higher amount of Ag had a smaller crystallite size and higher values of deformation and lattice parameter.

Nanohardness values up to 8 GPa were obtained for the stainless steel coatings, corresponding to a significant increase in the hardness compared to the hardness of the AISI 316L steel used as substrate. The coatings with Ag and deposited in a reactive atmosphere exhibited a higher degree of hardness, which can be attributed to the fact that the use of nitrogen tends to stabilize the austenitic phase of stainless steel and cause an increase in the lattice parameter and the percentage of deformation, due to the supersaturation of nitrogen in the austenitic structure.

The COF in the produced coatings was reduced in comparison with the substrate. In the coatings deposited in a reactive atmosphere, there was a tendency to decrease the COF with an increase in silver content. This behaviour can be attributed to a good solid lubricant, Ag, which allows lubrication of the wear tracks of the film and friction pairs, so that the sliding between the two surfaces tends to decrease the friction coefficient of the coating.

Finally, the wear rates in the produced coatings were reduced in comparison with the substrate, which is associated with the significant increase in the hardness of the coatings. The coatings deposited with lower Ag content (Ar0Ag and ArN0Ag) have a lower value of the wear rate. The decrease in the wear resistance with the increase of Ag is possibly due to an increase in the fragility of the material, loss of adhesion, Ag aggregates, or debris formed on the wear track.

Author Contributions: C.L.E.P., A.A.C.R. and J.J.O. conceived and designed the experiments; C.L.E.P. performed the experiments; C.L.E.P., A.A.C.R. and J.J.O. wrote the paper.

References

1. Antunes, R.A.; Rodas, A.C.D.; Lima, N.B.; Higa, O.Z.; Costa, I. Study of the corrosion resistance and in vitro biocompatibility of PVD TiCN-coated AISI 316 L austenitic stainless steel for orthopedic applications. *Surf. Coat. Technol.* **2010**, *205*, 2074–2081. [CrossRef]

2. Parsapour, A.; Khorasani, S.N.; Fathi, M.H. Effect of surface treatment and metallic coating on corrosion behavior and biocompatibility of surgical 316L stainless steel implant. *J. Mater. Sci. Technol.* **2012**, *28*, 125–131. [CrossRef]

3. Pareja López, A.N.D.R.É.S.; García García, C.P.; Abad Mejía, P.J.; Márquez Fernández, M.E. Citotoxic and genotoxic study of in vitro released products of stainless steel 316L with bioactive ceramic coatings. *Iatreia* **2007**, *20*, 12–20. (In Spanish)

4. Gopi, D.; Ramya, S.; Rajeswari, D.; Kavitha, L. Corrosion protection performance of porous strontium hydroxyapatite coating on polypyrrole coated 316L stainless steel. *Colloids Surf. B* **2013**, *107*, 130–136. [CrossRef] [PubMed]

5. Anghelina, F.V.; Ungureanu, D.N.; Bratu, V.; Popescu, I.N.; Rusanescu, C.O. Fine structure analysis of biocompatible ceramic materials based hydroxyapatite and metallic biomaterials 316L. *Appl. Surf. Sci.* **2013**, *285*, 65–71. [CrossRef]

6. Kannan, S.; Balamurugan, A.; Rajeswari, S. Hydroxyapatite coatings on sulfuric acid treated type 316L SS and its electrochemical behaviour in Ringer's solution. *Mater. Lett.* **2003**, *57*, 2382–2389. [CrossRef]

7. Kuroda, D.; Hiromoto, S.; Hanawa, T.; Katada, Y. Corrosion behavior of nickel-free high nitrogen austenitic stainless steel in simulated biological environments. *Mater. Trans.* **2002**, *43*, 3100–3104. [CrossRef]

8. Wang, L.; Zhao, X.; Ding, M.H.; Zheng, H.; Zhang, H.S.; Zhang, B.; Li, X.Q.; Wu, G.Y. Surface modification of biomedical AISI 316L stainless steel with zirconium carbonitride coatings. *Appl. Surf. Sci.* **2015**, *340*, 113–119. [CrossRef]

9. Schneider, J.M.; Rebholz, C.; Voevodin, A.A.; Leyland, A.; Matthews, A. Deposition and characterization of nitrogen containing stainless steel coatings prepared by reactive magnetron sputtering. *Vacuum* **1996**, *47*, 1077–1080. [CrossRef]

10. Kappaganthu, S.R.; Sun, Y. Formation of an MN-type cubic nitride phase in reactively sputtered stainless steel-nitrogen films. *J. Cryst. Growth* **2004**, *267*, 385–393. [CrossRef]

11. Kappaganthu, S.R.; Sun, Y. Influence of sputter deposition conditions on phase evolution in nitrogen-doped stainless steel films. *Surf. Coat. Technol.* **2005**, *198*, 59–63. [CrossRef]

12. Campoccia, D.; Montanaro, L.; Arciola, C.R. A review of the biomaterials technologies for infection-resistant surfaces. *Biomaterials* **2013**, *34*, 8533–8554. [CrossRef] [PubMed]

13. Ávalos, A.; Haza, A.I.; Morales, P. Nanopartículas de plata: Aplicaciones y riesgos tóxicos para la salud humana y el medio ambiente. *Rev. Complut. Cienc. Vet.* **2013**, *7*, 1–23. [CrossRef]

14. Taglietti, A.; Arciola, C.R.; D'Agostino, A.; Dacarro, G.; Montanaro, L.; Campoccia, D.; Cucca, L.; Vercellino, M.; Poggi, A.; Pallavicini, P.; et al. Antibiofilm activity of a monolayer of silver nanoparticles anchored to an amino-silanized glass surface. *Biomaterials* **2014**, *35*, 1779–1788. [CrossRef] [PubMed]

15. Velasco, S.C.; Cavaleiro, A.; Carvalho, S. Functional properties of ceramic-Ag nanocomposite coatings produced by magnetron sputtering. *Prog. Mater. Sci.* **2016**, *84*, 158–191. [CrossRef]

16. Manninen, N.K.; Ribeiro, F.; Escudeiro, A.; Polcar, T.; Carvalho, S.; Cavaleiro, A. Influence of Ag content on mechanical and tribological behavior of DLC coatings. *Surf. Coat. Technol.* **2013**, *232*, 440–446. [CrossRef]

17. Dang, C.; Li, J.; Wang, Y.; Yang, Y.; Wang, Y.; Chen, J. Influence of Ag contents on structure and tribological properties of TiSiN-Ag nanocomposite coatings on Ti–6Al–4V. *Appl. Surf. Sci.* **2017**, *394*, 613–624. [CrossRef]

18. Macías, H.A.; Yate, L.; Coy, L.E.; Olaya, J.; Aperador, W. Effect of nitrogen flow ratio on microstructure, mechanical and tribological properties of TiWSiN$_x$ thin film deposited by magnetron co-sputtering. *Appl. Surf. Sci.* **2018**, *456*, 445–456. [CrossRef]

19. *ASTM G99 Standard Test Method for Wear Testing with a Pin-on-Disk Apparatus*; ASTM International: West Conshohocken, PA, USA, 2006.

20. Ju, H.; He, S.; Yu, L.; Asempah, I.; Xu, J. The improvement of oxidation resistance, mechanical and tribological properties of W$_2$N films by doping silicon. *Surf. Coat. Technol.* **2017**, *317*, 158–165. [CrossRef]

21. Sánchez-López, J.C.; Abad, M.D.; Carvalho, I.; Galindo, R.E.; Benito, N.; Ribeiro, S.; Henriquese, M.; Cavaleirof, A.; Carvalho, S. Influence of silver content on the tribomechanical behavior on Ag-TiCN bioactive coatings. *Surf. Coat. Technol.* **2012**, *206*, 2192–2198. [CrossRef]

22. Bai, L.; Hang, R.; Gao, A.; Zhang, X.; Huang, X.; Wang, Y.; Tang, B.; Zhao, L.; Chu, P.K. Nanostructured titanium–silver coatings with good antibacterial activity and cytocompatibility fabricated by one-step magnetron sputtering. *Appl. Surf. Sci.* **2015**, *355*, 32–44. [CrossRef]

23. Aouadi, S.M.; Debessai, M.; Filip, P. Zirconium nitride/silver nanocomposite structures for biomedical applications. *J. Vac. Sci. Technol. B* **2004**, *22*, 1134–1140. [CrossRef]

24. Ferreri, I.; Lopes, V.; Tavares, C.J.; Cavaleiro, A.; Carvalho, S. Study of the effect of the silver content on the structural and mechanical behavior of Ag–ZrCN coatings for orthopedic prostheses. *Mater. Sci. Eng. C* **2014**, *42*, 782–790. [CrossRef] [PubMed]

25. Dahm, K.L.; Dearnley, P.A. On the nature, properties and wear response of s-phase (nitrogen-alloyed stainless steel) coatings on AISI 316L. *Proc. Inst. Mech. Eng. Part L J. Mater. Des. Appl.* **2000**, *214*, 181–198.

26. Bourjot, A.; Foos, M.; Frantz, C. Basic properties of sputtered 310 stainless steel—Nitrogen coatings. In *Metallurgical Coatings and Thin Films 1990*; Sartwell, B.D., Zemel, J.N., McGuire, G.E., Bresnock, F.N., Eds.; Elsevier: London, UK, 1990; pp. 533–542.

27. Thornton, J.A. The microstructure of sputter-deposited coatings. *J. Vac. Sci. Technol. A* **1986**, *4*, 3059–3065. [CrossRef]

28. Kelly, P.J.; Li, H.; Benson, P.S.; Whitehead, K.A.; Verran, J.; Arnell, R.D.; Iordanova, I. Comparison of the tribological and antimicrobial properties of CrN/Ag, ZrN/Ag, TiN/Ag, and TiN/Cu nanocomposite coatings. *Surf. Coat. Technol.* **2010**, *205*, 1606–1610. [CrossRef]

29. Leyland, A.; Matthews, A. On the significance of the H/E ratio in wear control: A nanocomposite coating approach to optimised tribological behaviour. *Wear* **2000**, *246*, 1–11. [CrossRef]

30. Buršík, J.; Buršíková, V.; Souček, P.; Zábranský, L.; Vašina, P. Characterization of Ta-BC nanostructured hard coatings. *IOP Conf. Ser. Mater. Sci. Eng.* **2017**, *175*, 012020. [CrossRef]

31. Pöhl, F.; Hardes, C.; Theisen, W. Scratch behavior of soft metallic materials. *AIMS Mater. Sci.* **2016**, *3*, 390–403. [CrossRef]

32. Tschiptschin, A.P.; Garzon, C.M.; Lopez, D.M. Scratch resistance of high nitrogen austenitic stainless steels. In *Tribology and Interface Engineering Series*; Sinha, S., Ed.; Elsevier: Amsterdam, The Netherlands, 2006; Volume 51, pp. 280–293.

33. *ASTM C1624-05 Standard Test Method for Adhesion Strength and Mechanical Failure Modes of Ceramic Coatings by Quantitative Single Point Scratch Testing*; ASTM International: West Conshohocken, PA, USA, 2005.

34. Mo, J.L.; Zhu, M.H. Tribological oxidation behaviour of PVD hard coatings. *Tribol. Int.* **2009**, *42*, 1758–1764. [CrossRef]

35. Yu, X.; Qin, Y.; Wang, C.B.; Yang, Y.Q.; Ma, X.C. Effects of nanocrystalline silver incorporation on sliding tribological properties of Ag-containing diamond-like carbon films in multi-ion beam assisted deposition. *Vacuum* **2013**, *89*, 82–85. [CrossRef]

36. Ju, H.; Yu, D.; Yu, L.; Ding, N.; Xu, J.; Zhang, X.; Zheng, Y.; Yang, L.; He, X. The influence of Ag contents on the microstructure, mechanical and tribological properties of ZrN-Ag films. *Vacuum* **2018**, *148*, 54–61. [CrossRef]